



UNIVERSITAT
POLITÈCNICA
DE VALÈNCIA


Escuela Técnica Superior de Ingeniería del Diseño



**Grainger College
of Engineering**
UNIVERSITY OF ILLINOIS URBANA-CHAMPAIGN

Bachelor's thesis

Non-Invasive Crater Measurements with Photogrammetry Techniques

Paloma Planelles Gironés

Degree of Bachelor of Science in Aerospace Engineering

Supervised by

Laura Villafañe Roca
Andrés Omar Tiseira Izaguirre

Academic Year 2021/22

Abstract

The study of aerodynamic and granular dynamics phenomena occurring during the propulsive landing of a spacecraft on a planetary surface is of vital importance for future missions to the Moon and Mars. In this project, a systematic way of obtaining three-dimensional measurements of a crater in a glass microsphere regolith simulant is described. The glass microspheres have a mean particle diameter of 105 μm and a standard deviation of 17 μm , and are in a 33 cm \times 18.4 cm \times 10 cm box. The crater is formed with a cylindrical cup. The crater depth, radius, and volume are calculated from a series of pictures using the software RealityCapture. A preliminary test case reconstructing a bottle with the software is performed before the test case. To boost the reconstruction a laser sheet is placed across the crater and the images are edited with Lightroom to enhance the contrast. The results prove that the measurement can be used to study the crater formed in the granular media bed during a plume-surface interaction experiment. This could bring additional information on plume-surface interaction processes.

Keywords: Plume-Surface Interactions, granular media, RealityCapture, control points, 3D reconstruction

Contents

1	Introduction	1
2	Photogrammetry Background	3
2.1	History	3
2.1.1	Plane table photogrammetry	4
2.1.2	Analog photogrammetry	4
2.1.3	Analytical photogrammetry	6
2.1.4	Digital photogrammetry	6
2.2	Photogrammetry used for PSI studies	7
3	Experimental Method	9
3.1	Materials used	9
3.2	Data acquisition	10
3.3	Data processing	10
3.3.1	Lightroom	10
3.3.2	RealityCapture	10
3.4	Preliminary test case	11
3.5	Test case	13
4	Conclusions	20
5	Bibliography	21

List of Figures

3.1	Ballotini glass microspheres.	9
3.2	Two of the images taken of the bottle for the future reconstruction. . .	12
3.3	Point cloud of bottle reconstruction with the camera positions.	12
3.4	Closer view of the cloud point reconstruction of the bottle.	13
3.5	Post-experiment craters obtained by Rasmont et al. [39].	14
3.6	Crater creation process with a cup.	14
3.7	Crater creation process with a cup.	15
3.8	Change in image after correction with Lightroom.	16
3.9	Point cloud of crater reconstruction.	16
3.10	Views of the cloud point reconstruction of the crater.	17
3.11	Points 0 and 1 on the point cloud.	17
3.12	Points 0, 1, 2, 7 and 10 location on an image.	18

List of Tables

3.1	Pre-processing in Adobe Lightroom	15
3.2	Points 0 and 1 coordinates calculated by RealityCapture in cm.	17
3.3	Points 2, 7 and 10 position in local coordinate system in cm.	18
3.4	Points 2, 7 and 10 position with respect to point 7 in cm.	19

1. Introduction

The impingement of hot rocket exhaust on the regolith of planetary bodies generates an environment characterized by the plume flow physics, cratering physics and ejecta dynamics [33]. Plume-surface interaction (PSI) is the discipline that studies the gas-soil erosion process under a supersonic jet [35]. The research and experience have shown that PSI is a challenge for missions consisting of launching or landing rockets on planetary bodies [35] [36].

The ejected material, due to the high velocity jet, can damage nearby scientific material, and form a dust cloud capable of blocking visibility. These conditions put the lander at risk. That is why understanding and predicting plume-surface interactions are of vital importance for future manned missions to the Moon or Mars and those that require multiple spacecraft within short distances of one another [36].

Even though the Apollo space program was a success, it experienced some minor risks and problems from PSI [47]. The Apollo 12 and 15 missions in particular showcase two situations that are useful case studies for PSI [35].

With the Apollo 12 mission effects of the PSI ejecta were noted. The exhaust gases can kick up rocks, gravel, soil and dust, damaging nearby hardware. The Surveyor III spacecraft, which was less than 200 m away from the landing site of the Apollo 12 lunar module, showed sandblasted hardware and micro-crates on its surface [35].

During the Apollo 15, the particles created a dust cloud that blocked visibility. The astronauts were not able to see that they were landing on the rim of a crater, so the Lunar Module tilted backwards 11 degrees until it was in equilibrium [35]. If the Lunar Module had been tilted more than 12 degrees, the astronauts would not have been able to lift-off [47]. This showed that the particles raised in the air can block visibility, putting the lander at risk.

There are five cratering mechanisms known to date. The first three were discovered and defined before the Apollo missions.

1. Viscous erosion (VE): the particles are moved tangentially to the surface along the top layer of grains due to the free flow in the boundary layer above the sand.
2. Bearing capacity failure (BCF): this happens when the stagnation pressure of the gas directly beneath the jet surpasses the bearing capacity of the soil, mechanically forcing it downward. This forms a crater under the jet.
3. Diffused gas eruption (DGE): this mechanism considers gas diffusion as a single soil-moving mechanism. Radial diffusion of pressure blows out a toroidal region around the exhaust jet.
4. Diffusion-driven shearing (DDS): the drag force of gas diffusing through the sand creates a sufficient body-force distributed throughout the sand, to setup a stress state that exceeds the soil's shear strength, initiating shearing.

5. Diffusive gas explosive erosion (DGEE): caused by supersonic pulsed jets impinging on porous soils in tenuous atmospheres. The localized fluidization of soil along with the formation and propagation of cyclic and radial granular shock waves give the explosive nature to this erosion process [34]. This occurs only when a rocket engine is ignited over soil. The impinging gas sends a shockwave into the soil prior to the formation of standoff shock [35].

The goal is to reliably reconstruct the 3d shape of the crater from a series of pictures using the software RealityCapture. This paper is structured as follows. First, an overview of photogrammetry is carried out with its main developments. Later, the experimental method is described. And, finally, conclusions and expectations for future work are discussed.

2. Photogrammetry Background

Photogrammetry is the art, science and technology of providing reliable information about the physical traits of objects from photographs. The main objective is to associate pixel positions, measured by the sensor, as accurately as possible to the actual position on the object [26]. It is a continuously developing technology that encapsulates many principles and techniques that have a wide range of complexity [1].

This technique is widely used in different areas such as geology, forestry, agriculture, design, construction, environmental studies, military intelligence, medicine and much more.

Photogrammetry needs two main items: the concept of image geometry, and the availability of a sensor system. The sensor system allows us to obtain the image [27]. Due to perspective or movements, there may be distortions caused acquiring the data. Rectifying an image is the process of removing deformations with the camera specifications and control points [26]. They are used in the experimental method (Section 3), therefore it is important to provide their definition. Control points are well defined points in the photograph that are easy to find and accessible on the object. They are used to do ground checks that determine the geometric relationship between point measurements in the photographs and the true location.

2.1. History

Photogrammetry is a technology that has been around for a long time. Its foundations date back to 1480, when Leonardo da Vinci stated the basis of perspective. The correlation between projective geometry and photogrammetry was first developed by R. Sturms and Guido Hauck in Germany in 1883 [7]. The first photograph was taken in 1826 by Joseph Nicéphore Niépce [45]. It was in black and white and needed eight hours of exposure. But the practice of photogrammetry could not occur until a practical photographic process was developed. It wasn't until 1839 that the photographic process was publicly available with the invention of the Daguerreotype by Louis Jacques Mandé Daguerre [37].

With the invention of the Daguerreotype, geodesist Dominique François Jean Arago proposed the use of photogrammetry to the French Arts and Science Academy in 1840. From then, the evolution of photogrammetry has followed four development cycles according to Konecny [27]:

1. Plane table photogrammetry (from 1850 to 1900).
2. Analog photogrammetry (from 1900 to 1960).
3. Analytical photogrammetry (from 1960 to 2010).
4. Digital photogrammetry (from 2010 to present).

2.1.1 Plane table photogrammetry

Colonel Laussedat was the first person to use a photograph for topographic purposes. He made a map of Paris with the images he took from the roofs of the city. This marks the beginning of the first development cycle: Plane table photogrammetry. It was an auxiliary survey method. The photographs were only used as a tool to obtain horizontal and vertical directions faster [27]. Laussedat is considered the “Father of Photogrammetry”. He tried aerial photography first with a string of kites in 1858, and later with balloons. In fact, he is the first person to have captured an image from a balloon. He later gave up, due to the difficulty of taking enough photographs to cover all the area from only one air station [7].

Gaspard Felix Tournachon, known as Nadar, was the first person to use the hot-air-balloon as an aerial platform. He photographed Paris in 1858, and in 1859 Napoleon ordered him to map out the enemy lines to prepare for the battle of Solferino.

An important improvement on photography was the design of the photogoniometer in 1865 by Paulo Ignazio Pietro Porro. The application of this development improves lens distortion. In the US, Cornele B. Adams obtained a patent for his “Method of Photogrammetry”. His approach consisted of taking two aerial photos of the same area with a camera from two positions of a balloon [2]. Adams invented radial line triangulation in an attempt to apply the principles of plane table photogrammetry to balloon photogrammetry [27].

In 1893, Dr Albrecht Meydenbauer used the term “photogrammetry” for the first time. He is renowned for his architectural studies using photogrammetry. He designed a camera with a device for aligning the camera axis and permanently mounted lens. With this camera, he performed the topographic map of Freyburg, Germany, and the structural drawing of St. Mary’s Church. [7].

Meydenbauer’s method used the approach of the time. The photograph was used to map the terrain by intersection and directions from ground control points that were graphically plotted from the representation.

Plane table photogrammetry also proved to be useful for the survey of historical monuments, expeditions and archaeology.

2.1.2 Analog photogrammetry

The second developing cycle started with two important events: the wide-spread use of stereoscopy and the development of the airplane by the Wright brothers in 1903 [7]. This cycle is characterized by the creation of a professional photogrammetrist to carry out analog photogrammetry, and the improvement of the technique that was exclusively used for topographic mapping [27].

Edouard-Gaston Deville developed in 1895, the first instrument for stereo-observation of overlapping photographs [27]. With it, details could be interpreted and traced, but its complexity resulted in little use. He succeeded in sketching the map of the Canadian Rocky Mountains. For the mapping, he used a camera and theodolite mounted on the same tripod. A theodolite is, according to the Collins English Dictionary [11], “a surveying instrument for measuring horizontal and vertical angles, consisting of a

small tripod-mounted telescope that is free to move in both the horizontal and vertical planes.”

The process was very difficult to perform and it was also tedious. For these reasons, photogrammetry was only used in situations where conventional plane table mapping was either too difficult or impractical [7].

Sebastian Finsterwalder established the real foundations of analytical photogrammetry in a series of papers published at the end of the 19th century [12].

Dr. Carl Pulfrich built the first stereocomparator in 1901, in Germany. It measured image coordinates, introducing the floating mark [27]. At the same time, in South Africa, Dr. Henry George Fourcade developed a similar stereocomparator. What made them different is that Fourcade used grid plates instead of x and y coordinates [7]. The stereocomparator was used to map the mountain region in Tyrol, where access was difficult and dangerous. It evolved into the stereautograph for terrestrial photographs. This was developed by Eduard Von Orel with the help of Pulfrich, and the Aerokartograph for aerial photographs by Hegershoff [12]. The stereautograph traced elevation contours directly for the first time. It also brought practicability to the use of terrestrial photogrammetry in the mountain, a method which is still in use [7].

The rapid technological development of analog photogrammetry required the formation of a discipline. The Society of Photogrammetry was formed in Vienna in 1907, and another one in Germany in 1909 with the same name. With two national societies, the International Society was created by Dolezal in 1910. Other countries joined and in 1913, Vienna held the First International Congress of Photogrammetry. World War I disrupted the society’s activities.

During World War I (1914-1918), the use of aerial photography increased thanks to the development of an aerial survey camera in 1915 by Oskar Messter. The camera could take vertical photographs with a regular overlap [27]

The foundation of the theory of analog restitution and its orientation was developed by Otto von Gruber in 1924. He derived the projective equations and their differentials, which are fundamental in analytical photogrammetry [7]. He also made the first attempts on spatial aerial triangulation.

Theodor Scheimpflug developed, in 1896, the principles for rectification. It was not until 1934 that it was possible to build rectifiers according to his theory thanks to Wild and Zeiss.

Sherman Mills Fairchild discovered, during World War I, the problems of image distortion on the aerial cameras used at the time. He developed a between-the-lens shutter that improved the quality of the images. He created Fairchild Aerial Surveys to provide photogrammetry services. His cameras were used on the Explorer II flights and in the Apollo missions for mapping the moon’s surface [48]. Aerial photogrammetry became a decisive tool for the United States and USSR to win World War II.

2.1.3 Analytical photogrammetry

The invention of the electronic computer by Zuse in Germany in 1941, and independently by Aitken in the US in 1943 initiated a new development boost after 1960. The third cycle of photogrammetric development, analytical photogrammetry, initiated with the use of the computer. [7]. Analytical photogrammetry is “a term used to describe the rigorous mathematical calculation of coordinates of points in object space based upon camera parameters, measured photo coordinates, and ground control. It generally involves the solution of large, complex systems of redundant equations by the method of least squares” [50].

In 1947, Ralph O. Anderson devised a semi-analytical approach for analytical control. In the early 1950s, Everett Meritt developed a series of “analytical solutions for camera calibration, space resection, interior and exterior orientation, relative and absolute orientation of stereo pairs, and analytical control extension” [12]. In 1953, Dr Hellmut Schmid defined the principles of modern multi-station analytical photogrammetry. His work presents “a correct least squares solution, simultaneous solution of any number of photographs and a complete study of error propagation” [12]. He used matrix notation, which now is a standard for analytical analysis. With the collaboration of Duane Brown, they were able to apply analytical photogrammetry to practical purposes.

Significant technological developments in analytical photogrammetry were carried out during the 1960s and 1970s. This led to a large rise in the application of analytical photogrammetry in different fields, during the 1980s [54]. In 1961 Duane Brown managed to adjust large photogrammetric blocks with self-calibration. This improved accuracy and reliability of photogrammetric adjustment. He also worked on taking photogrammetry from a tool requiring highly-trained professionals, to a turn-key system that could be used directly from the client. Houssan Mahmoud (Sam) Karara managed to perform direct transformations from comparator measurements to object-space coordinates without camera calibration data [7].

2.1.4 Digital photogrammetry

A shift from analytical to digital photogrammetry has been taking place since 1990. This transition was caused by the desire to be more efficient through the automation of mapping procedures [41].

In 1957, Gilbert Louis Hobrough demonstrated the concept of image correlation. In 1967, he developed an automated orthophotographic system that used correlation between stereo images. Different digital photogrammetric workstations have been developed since then. Airbus Defence and Space in France released PIXEL FACTORY. It is capable of processing a vast number of images to produce 3-D cartographic end products. [54].

The advancements that have taken place since the end of the 20th century until now have enabled photogrammetry to become the most accurate and efficient method for mapping and generating topographic information [53]. Photogrammetry has been used for non-topographic purposes for years in the following fields: engineering research, astronomy and medicine, amongst others. However, the practical use in those areas has

been limited because of the slow development of photogrammetry for those applications [20][32].

A digital image is a “computer-compatible pictorial rendition in which the image is divided into a fine grid of picture elements, or pixels” [51]. The image is made up of an array of integers, the digital numbers, that specify the gray level at a particular element. When an image has many thousands or millions of pixels, it looks like that of a continuous-tone picture.

Geometric resolution is a relevant characteristic of discrete sampling of an image. It refers to the physical size of each individual pixel that constitutes the image. Smaller pixel size corresponds to a higher geometric resolution. Another important characteristic of digital images is radiometric resolution. Radiometric resolution can be divided into quantization and spectral resolution. Quantization resolution is the number of discrete levels in which the original electromagnetic energy is converted. Those levels correspond to the gray levels. The higher quantization resolution, the more accurate digital representation of the analog signal [52]. Spectral resolution describes the wavelength intervals. It determines the colors in the image. In a black and white image, there is only one spectral band covering the entire visible range from violet through red.

The photogrammetric reconstruction of 3D objects is presently accomplished based on point clouds generated by dense image matching techniques [15].

2.2. Photogrammetry used for PSI studies

Optical diagnosis has been vital for understanding PSI. Videos from the Apollo missions were used, to try to determine the soil ejections angles [35].

Clark and Behringer [8] used a thin, transparent box to simulate quasi-two-dimensional behavior of a crater formation. This setup facilitated optical access, in which a camera was used to take images of the crater formation process. Those images were then studied to determine shape and depth.

Another experimental setup was developed by Robert Haehnel [19] and has been commonly used since then [18][36][22][17][29][30]. It consisted of a specially-constructed box with a window that allowed viewing of the crater. The top edge of the window was beveled and aligned with the symmetry plane of the impinging jet [19].

Similarly to Haehnel’s technique, Mehta et al. [34] created a quarter space technique to study the effect of exhaust impingement on the Phoenix engines on Mars. The setup included two transparent baffles that simulated the planes of symmetry with neighboring thrusters to visualize the erosion process through still and high speed imaging.

Both the split plate and quarter space techniques are useful, but they are also intrusive. The experiments were conducted in flow-intrusive, partial-domain experiments. The techniques can potentially alter the physics of the crater formation process [17][30].

Photogrammetry is first used by Stubbs et al. [43] to study PSI. Their experimental setup consisted of a test section enclosed by three clear panels, and one opaque panel that worked as background. High-speed stereo image pairs were obtained and stereo-photogrammetry was implemented with the photographs taken. They obtained a 3-D point cloud reconstruction of the crater formation process from the data.

3. Experimental Method

The material used as regolith simulant was glass microspheres. Some color correction was done on the images with Lightroom to obtain better results. The software selected to process the images and obtain a 3D model from the images was RealityCapture. First, the program was tested with a bottle that was reconstructed with a point cloud. Then, the reconstruction of the Ballotini glass microspheres was performed, to simulate its intended usage.

3.1. Materials used

The material used to make the regolith simulant is Ballotini glass microspheres. The particles have a density $\rho = 2500 \text{ kg}\cdot\text{m}^{-3}$, a particle size distribution with a mean particle diameter of $D = 105 \text{ }\mu\text{m}$ and a standard deviation of $\sigma_D = 17 \text{ }\mu\text{m}$. [39]. These particles are typically used in industry for cleaning, deburring, finishing, and peening applications.

It is a very homogeneous material as can be seen in Figure 3.1a, which makes the photogrammetry process more complicated, because there are not enough contrasts within the pixels to generate the point cloud. There are examples of sand being processed with RealityCapture with good results with the sand's texture [5], although in this case the sand had more contrasts than the particles used. Despite this drawback, the material was chosen because the density is close to actual lunar and martial regolith, PSI with spherical particles is easier to analyze and model than actual sand or regolith, and the relatively narrow size distribution simplifies the PSI physics involved in the experiment carried out by Rasmont et al. [39]. In Figure 3.1b, the individual grains can be seen. This work is meant to eventually be applied to analyze the results of Rasmont and Al-Rashdan's experiments.

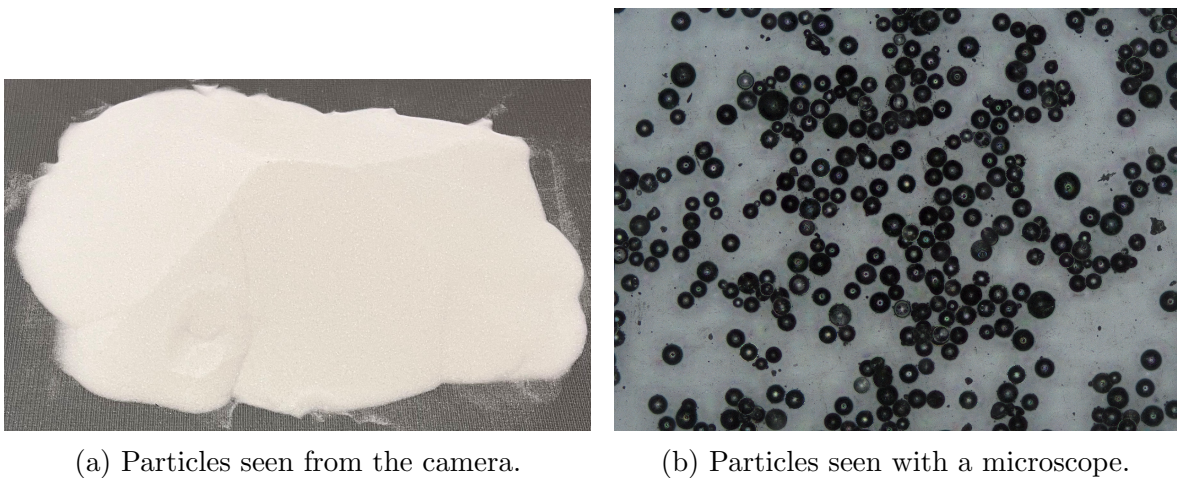


Figure 3.1: Ballotini glass microspheres.

3.2. Data acquisition

One of the most important parts of photogrammetry is the data acquisition step. Lighting should be even and diffused so there are not shadows [21]. The best camera arrangements to obtain good images for the data processing are low ISO (around 100) and low f/stop, between f8 and f11. This allows the camera to capture enough light and get a clean image with no regard of the background [21][28][13].

When taking the pictures, there must be an 80% overlap between one photograph and the next one. RealityCapture counts by seeing any feature from at least two (although there can be more) different angles. So the camera should be moved for every single shot with an angle bigger than 5° , but less than 30° . If the angle difference between images is less than 5° , errors arise in placing the tie point depthwise [13].

The settings on the cameras for both the preliminary test case and the test case had the contrast set to normal, as well as the saturation and sharpness.

3.3. Data processing

3.3.1 Lightroom

Lightroom is a creative image organization and image manipulation software developed by Adobe Inc [3]. It handles large amounts of photos, so it is very useful for photogrammetry, where a lot of images are taken that have to have the same properties (exposure, saturation, light, shadows, clarity).

Lightroom is a tool very commonly used in pre-processing to calibrate colors, improve contrast, and render consistency among all the images [31][9][16][23][49][38].

3.3.2 RealityCapture

RealityCapture is a European based digital photogrammetry program developed by Capturing Reality [24]. It is mostly used for art and architecture purposes, as well as full body scanning, gaming, surveying, mapping, visual effects and virtual reality.

The term “reality capture” refers to the collection of the best and most accurate data about real-world conditions, known as the “as-built” or “as-is condition.” The captured data is called the “point cloud” [4].

It is a quite new application on the market, but it has good reviews among users [15]. Even though it has yet to be critically evaluated in any academic publication, there have been several studies that situate its process time as the shortest compared to other public and commercial softwares [24][25][15]. The reason for shorter reconstruction process time is that RealityCapture uses loop-closing techniques based on SURF-based visual words [6] and tf-idf scores [42]. Most of the computations are performed by GPU cores [15].

In 2021, a study performed by Verykokou et al. [46] found the software Metashape to obtain faster results than RealityCapture, although RealityCapture was “still very fast,” and the solutions were comparable in terms of accuracy.

The photogrammetry reconstruction of 3D objects is performed based on point clouds produced by dense image matching techniques [15]. The point clouds generation is performed from large sets of unordered images [14][40]. When Reality Capture reconstructs a model, it tries to add the information collected from each photo into the currently existing model, called a component. Nevertheless, if the program is not able to figure out how the photo concerned contributes to the component, a second component is created. The forthcoming photos are compared to the original and the newly added component [10]. In this case, if the photos are not be aligned properly, a person must take the time to manually align the images properly adding by control points.

3.4. Preliminary test case

Before performing the test case with the Ballotini glass microspheres, a preliminary test case was performed to gauge RealityCapture and the amount of images needed and how they had to be taken for the specific software.

The camera used for this test was the rear camera of the Microsoft Surface Pro 6, which is a 8-megapixel camera. The advantages of this camera is that the balance of whites, ISO, shutter speed and f aperture can be manually chosen. The camera resolution is 2448×3264 . The images were taken without flash, with an ISO of 170, f/stop at 2, shutter time $1/33$ s and focal length of 30 mm. These are not the ideal settings mentioned in Section 3.2, because the camera and lighting were not good enough to set those. But they were enough to learn to use RealityCapture, and obtain results that demonstrated the reliability of the program to know that it could be further used.

There were some setbacks when acquiring the data. The proportions of the camera device, because the lens is at one side of it; and the Surface's size, because it was difficult to handle when taking pictures. Furthermore, the surface where the bottle was placed was too big in comparison to the bottle. This did not allow the bottle to occupy most of the available space in the image, which would have been better to get more information from the pictures. In the pictures taken, the background covers most of it, as can be seen in Figure 3.2a. Figure 3.2b shows a close up of one of the images in the batch used later for the reconstruction.

Two points can be found in Figure 3.2b. Those are two of the three artificially created control points that were added to the object to help with the Reconstruction. This makes it easier for RealityCapture, and can be used to align two or more components when the software is not able to associate all the images together.

With all the images taken and added to the RealityCapture Workflow, the image matching was performed using the alignment option with default settings. As mentioned before, much of the background could be seen in the photos, so it appeared in the point cloud reconstruction. Figure 3.3 shows the point cloud after the reconstruction region was reduced to only the bottle. The white dots appearing in the image are the different camera positions at which the images were taken. It can be noticed that they are very far from the object, as was mentioned before, which results in the reconstruction being too small.



(a) Example of image taken showing that most of it is background.



(b) Closed-up image where artificially added control points can be seen.

Figure 3.2: Two of the images taken of the bottle for the future reconstruction.

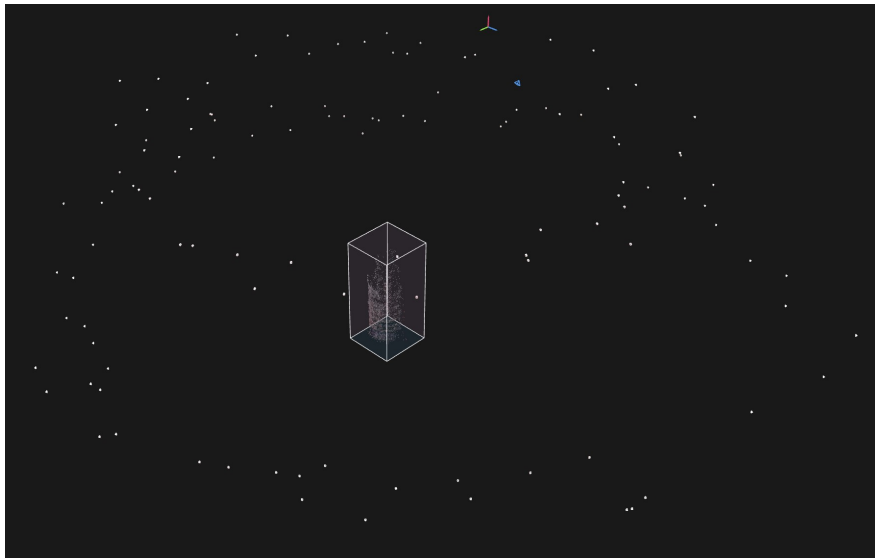


Figure 3.3: Point cloud of bottle reconstruction with the camera positions.

Figure 3.4 shows a closer look of the top, back and left view of the sparse cloud resulting from aligning the images. The control points are shown in the views as small blue circles. It can be noticed, especially from the top (Fig. 3.4a) and left (Fig. 3.4c) view that there is one part of the bottle with less tie points than the rest. The reason is that the bottle had a sticker around it that did not cover it completely. This can be seen in Figure 3.2. The part that is not covered has less tie points. This is probably

because that material is more homogeneous than the paper of the sticker.

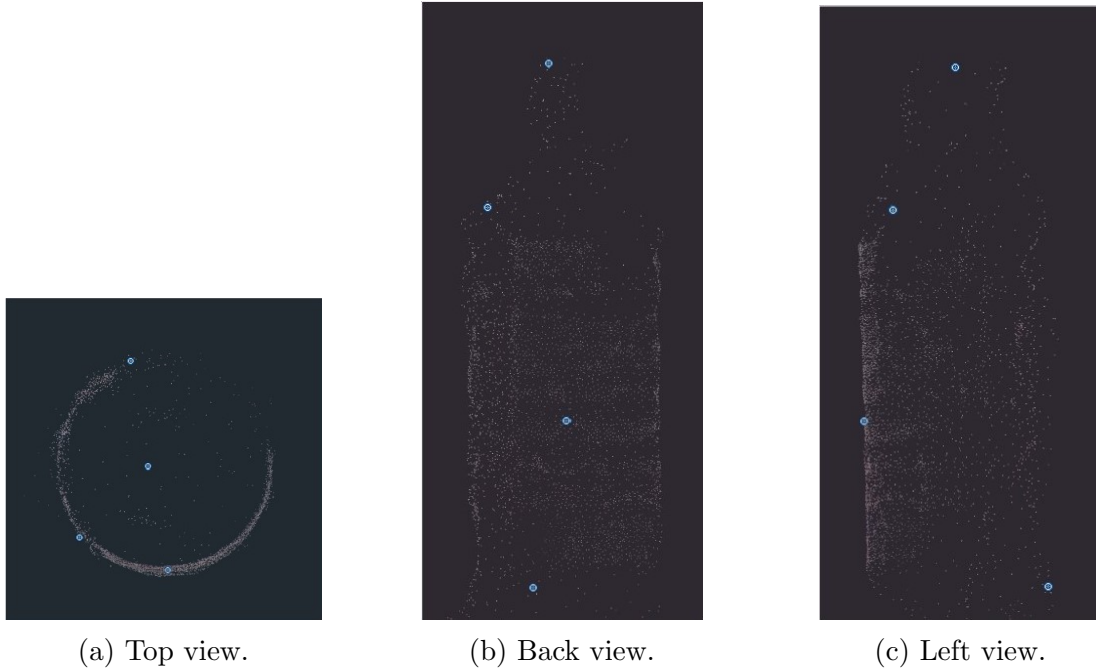


Figure 3.4: Closer view of the cloud point reconstruction of the bottle.

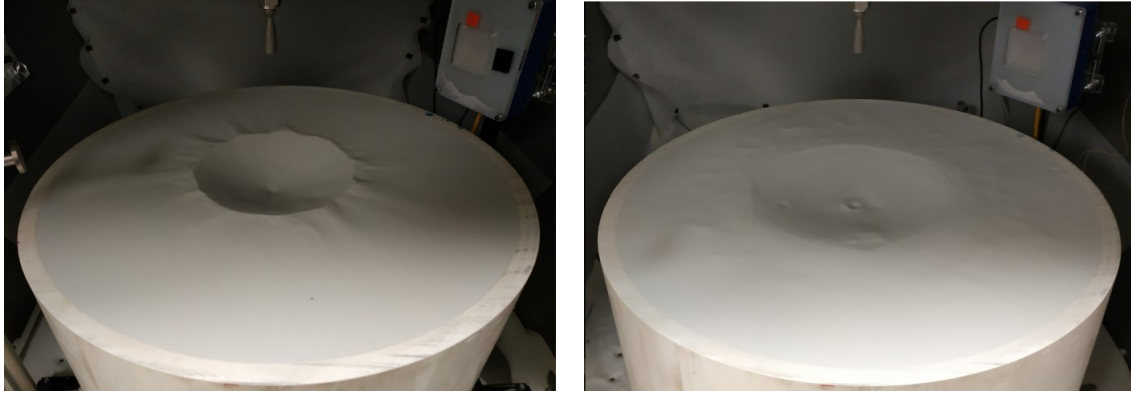
With the obtained point cloud, a mesh cannot be obtained because there are not enough points and they do not cover the whole object. Despite this, the artificially added control points are in the right position and their coordinates are given in Reality-Capture. Therefore, if it was possible to add something to the glass microspheres that acted as artificial control points, it would be possible to know the crater dimensions.

3.5. Test case

First, a setup that resembled the state of the regolith simulant. Figure 3.5 shows two different-looking craters that were obtained after the jet-impingement at different pressures to resemble the lunar case (Fig. 3.5a) and the martian case (Fig. 3.5b).

To obtain a crater that could be representative and comparable to the craters in Figure 3.5, the glass particles were deposited in a 33 cm \times 18.4 cm \times 10 cm plastic box and a hole resembling a crater was done with a plastic cup. The cup's diameter was $d = 5.8$ cm and was sunk 3.8 cm in the granular media. Figure 3.6 shows the crater creation process just mentioned.

There are black dots on the box edges (Fig. 3.6). These were painted on the box to work as control points. Apart from that, something needed to be added on the granular media to add some contrast in order to get more definition in the Point Cloud. For that, a linear laser was pointed towards the glass microspheres as shown in Figure 3.7.



(a) Crater showing streak-like structures.

(b) Crater without the structures.

Figure 3.5: Post-experiment craters obtained by Rasmont et al. [39].



Figure 3.6: Crater creation process with a cup.

The only laser available at the time of the test case performance was a point laser. To obtain a line, the laser was positioned pointing at a transparent, plastic pen in a way that the ray of light was reflected and became a line. The laser source and pen setup is shown in Figure 3.6.

Once the setup was ready, the next step was the data acquisition. For the test case, the camera used was the Canon IXUS 117 HS. It is automatic and has a resolution of 4000×3000 . The photos were taken with an ISO-100, $f2.8$, shutter time of $1/15$ s, focal length of 5 mm, and without flash.

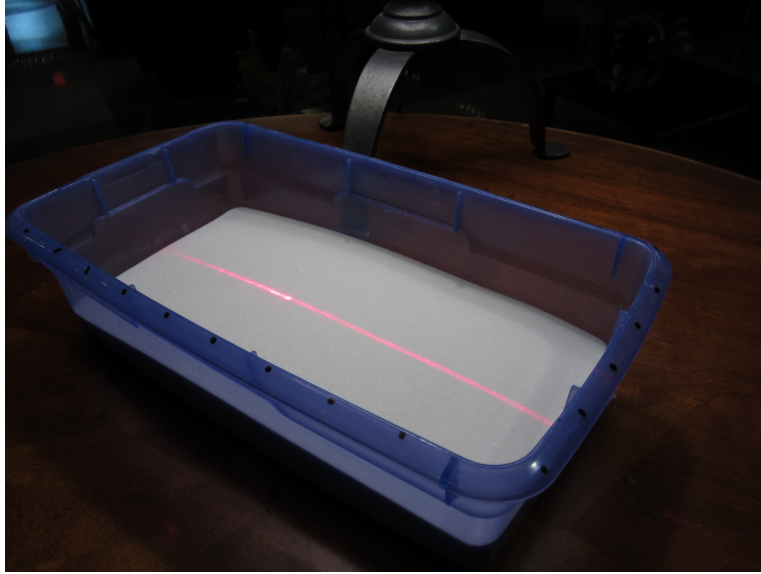


Figure 3.7: Crater creation process with a cup.

The data acquisition process was very similar to the one followed in Section 3.4, but more care was taken in having enough images from all the angles, and adding a correction to the images with Adobe Lightroom. When taking the pictures, an attempt of filling most of the frame with the box was done. This attempt is shown in Figures 3.7 and 3.8a. The images were taken moving around the box following the 80% rule explained in Section 3.2.

Filtering and pre-processing of photos is not always necessary, but can be used to retrieve 3D models that would otherwise be blurry or incomplete. In this case, it was done to improve contrast, especially on the edges and bottom of the crater. Table 3.1 shows the adjustments done to the images with Lightroom.

Options	Details
Exposure	+0.5
Highlights	-100
Shadows	+100
Whites	+20
Color temperature	-5
Clarity	+62
Noise Reduction	27

Table 3.1: Pre-processing in Adobe Lightroom

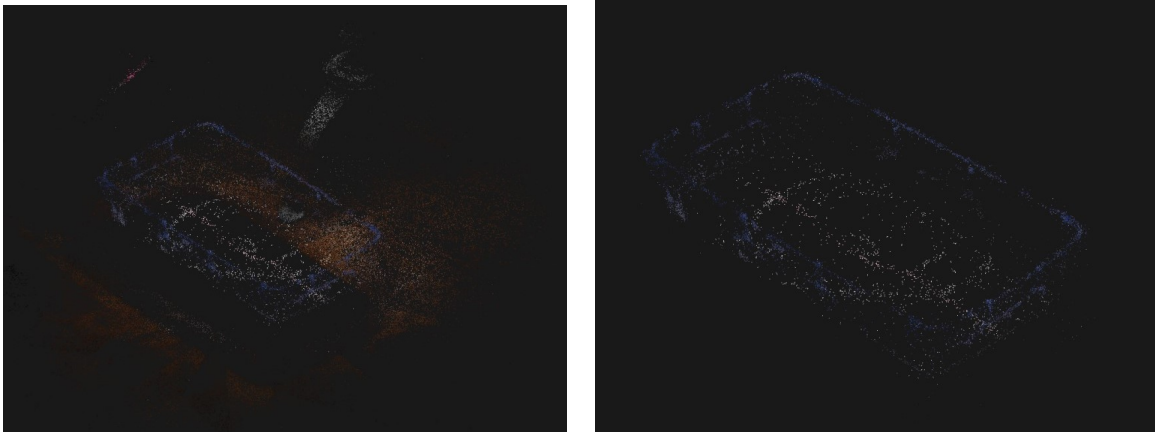
The result after the alterations is shown in Figure 3.8. At first glance, the main changes were that the background was more visible in the edited photo, and the glass microspheres did not look as white anymore. The color is not important since the main focus of the test case is to obtain a good 3D point cloud to take measurements. The background can be omitted by changing the reconstruction region later in RealityCapture, as was done in the preliminary test case (Section 3.4) with the bottle.



(a) Image before edition with Lightroom. (b) Image after edition with Lightroom.

Figure 3.8: Change in image after correction with Lightroom.

With the edited pictures in RealityCapture, the alignment was performed. The result obtained with this first alignment is shown in Figure 3.9a. There was a great deal of background, preventing a good assessment of the crater. So, as done at the preliminary test case, the reconstruction region was set to only the box volume, as shown in Figure 3.9b.

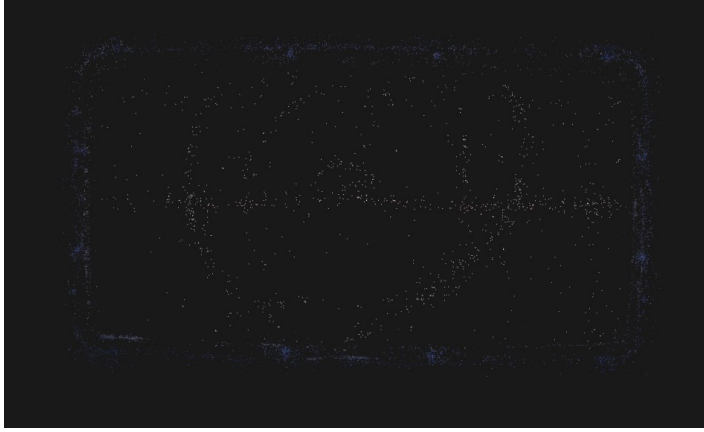


(a) With the background visible. (b) Without the background.

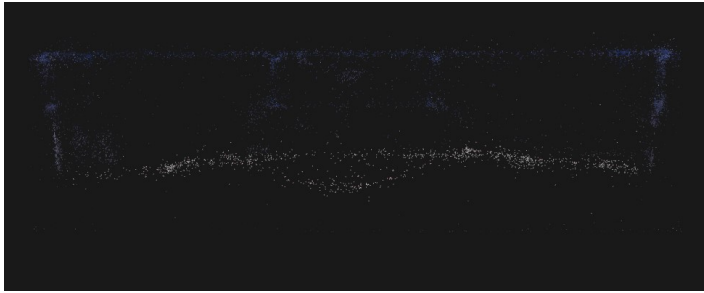
Figure 3.9: Point cloud of crater reconstruction.

Figure 3.10 shows the top, front and left view of the reconstruction region of the crater. Even though the cloud is not dense enough to cover all the surface, the edges of the crater and the depth. The slope can also be seen in Figure 3.10b.

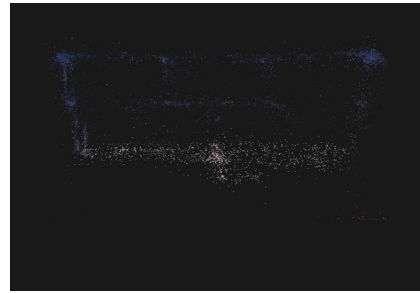
To calibrate the point cloud distances, two control points were added on one edge of the box with two painted black dots. The control points appear as “point 0” and “point 1” in Figure 3.11, and their coordinates are shown in Table 3.2.



(a) Top view.



(b) Front view.



(c) Left view.

Figure 3.10: Views of the cloud point reconstruction of the crater.

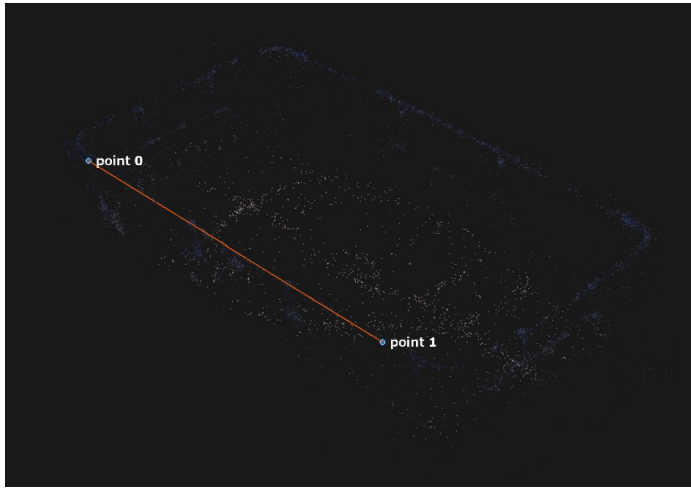


Figure 3.11: Points 0 and 1 on the point cloud.

Coordinate	Point 0	Point 1
x	-15.69	8.76
y	-20.34	-21.86
z	44.04	44.13

Table 3.2: Points 0 and 1 coordinates calculated by RealityCapture in cm.

It was unknown where the origin, or center of coordinates, is located. So the distance between the points was calculated both from the Software and from the box with a ruler. The points have been indicated in Figure 3.12.

The distance between point 0 and 1 measured with a ruler was 24.5 cm. While taking that measurement, it was noted that the box margin, even though it is not fully noticeable on the photographs, was not horizontal, but curved. That is why point 0 and 1 have different heights (z-coordinate in Table 3.2). The distance calculated from

the coordinates was 24.5 cm, the same as measured with the ruler. To calculate the distance, Equation 3.1 was followed.

$$d = \sqrt{(x_0 - x_1)^2 + (y_0 - y_1)^2 + (z_0 - z_1)^2} \quad (3.1)$$

This result shows that RealityCapture’s control points are the right position and distance from each other. With this, three more control points were added. Point 2 was situated in the middle of the interior of the crater. Point 7 is situated on the uppermost edge of the crater. And Point 10 is on the opposite side of point 7, with point 2 in between. The points can be seen in Figure 3.12.

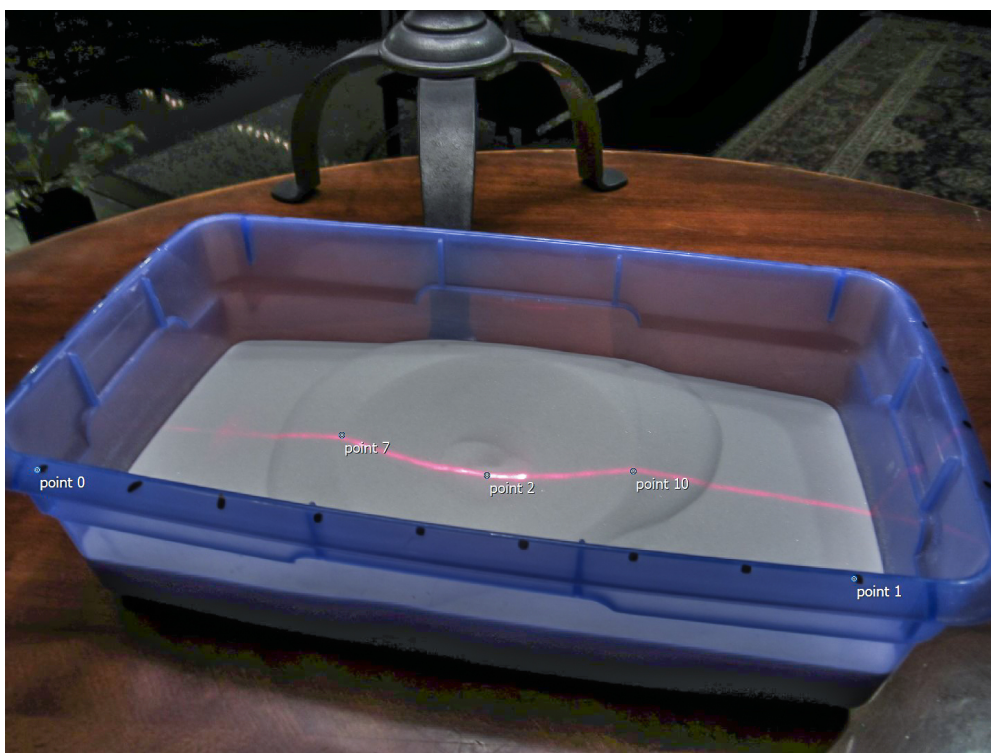


Figure 3.12: Points 0, 1, 2, 7 and 10 location on an image.

Tables 3.3 and 3.4 show the location of points 2, 7 and 10 in RealityCapture’s local coordinate system (Table 3.3) and with respect to point 7 (Table 3.4). So, with that, it can be determined that the crater has a width of 12.24 cm, a depth of 1.27 cm compared to point 7 and of 1.64 cm compared to point 10.

Coordinate	Point 7	Point 2	Point 10
x	-8.78	-2,53	3.46
y	-11.77	-12.16	-12.93
z	38.78	37.51	39.15

Table 3.3: Points 2, 7 and 10 position in local coordinate system in cm.

Coordinate	Point 7	Point 2	Point10
x	0	6.25	12.24
y	0	-0.40	-1.16
z	0	-1.27	0.37

Table 3.4: Points 2, 7 and 10 position with respect to point 7 in cm.

It was not possible to add control points on the material without laser, so the width perpendicular to the laser could not be calculated. There was only one laser available at the time of the test case performance. Furthermore, the box sides were too high, so they covered part of the particles in some pictures, and made shades that could have been prevented with a shorter box. The box walls covering parts of the crater, together with the lamp on one side of the box, led to less access to the crater with the camera. This produced a less detailed point cloud. Despite this, the test case has proven that photogrammetry applied with RealityCapture can be a reliable tool to reconstruct a 3-D point cloud of a crater formed after engine impingement.

The application of photogrammetry to reconstruct the post-experiment craters would have a different setup. It would be crucial to be able to access the granular media bed from all angles, as it is important to obtain images from all around it. It would also be necessary to use two lines of lasers instead of one. This way, more information about the crater could be determined. And the reconstruction would be improved, as the lasers would provide contrast with the rest of the particles and RealityCapture. Artificial control points could then be added to the granular media bed's edges for calibration purposes and a better result in RealityCapture.

4. Conclusions

In this study, a preliminary test case and a test case were performed to determine RealityCapture's usefulness for 3-D crater reconstructions for the study of PSI. The preliminary test case proved to give good results even without ideal lighting and camera conditions. The experience of the preliminary test case revealed the importance of photographing 360° around the object. It also exhibited that homogeneous and translucent materials are more difficult to reconstruct. The test case showed that control points can be utilized to counter the difficult reconstruction of homogeneous materials.

Even though the result obtained with RealityCapture was a scattered cloud point, adding control points at the right locations can be enough to determine plenty of information about the crater. In the test case, the depth and width was able to be determined. Future work could involve determining the crater's depth with respect to the surface surrounding the crater; not using the edges, as was done in Section 3.5. The crater's edge height, with respect to the surrounding surface, could also be calculated. For these two examples, only two more control points would be needed. Calculating the slope of the crater would also be possible. For that, several control points would have to be added, making sure that they were all within the same line. A linear regression of those control points could determine the slope.

It is true that the addition of control points is time consuming. They have to be added on every image. Even though RealityCapture automatically adds it to the rest of the photos, they need to be reviewed one by one. Despite this, they have proven to be helpful and give good results.

Photogrammetry has proved to be useful for a large amalgam of fields. As seen in Section 2.1, it takes time and research for it to become less time consuming and more automated. This paper, together with the work done by Stubbs et al. [43][44], demonstrates the utility and importance photogrammetry has and can continue to have in understanding and predicting plume surface interactions. The creation of new software and iterations of software for digital photogrammetry is inevitable, with changes, improvements, and new uses happening. Constant evaluation and re-evaluation of these programs is required to keep up with the best and most current digital photogrammetry practices.

5. Bibliography

- [1] James S. Aber, Irene Marzolff, and Johannes B. Ries. Chapter 3 - photogrammetry. In James S. Aber, Irene Marzolff, and Johannes B. Ries, editors, *Small-Format Aerial Photography*, pages 23–39. Elsevier, Amsterdam, 2010. ISBN 978-0-444-53260-2. doi: <https://doi.org/10.1016/B978-0-444-53260-2.10003-1>. URL <https://www.sciencedirect.com/science/article/pii/B9780444532602100031>.
- [2] Cornele B. Adams. *Method of photogrammetry*. U.S. Patent 510 758, December 12, 1893.
- [3] Adobe. Lightroom vs. photoshop: When to use each image editing program. URL <https://www.adobe.com/creativecloud/photography/lightroom-vs-photoshop.html>.
- [4] Avar Almukhtar, Zaid O. Saeed, Henry Abanda, and Joseph H. M. Tah. Reality capture of buildings using 3d laser scanners. *CivilEng*, 2(1):214–235, 2021. ISSN 2673-4109. doi: 10.3390/civileng2010012. URL <https://www.mdpi.com/2673-4109/2/1/12>.
- [5] Grzegorz Baran. The sand-photogrammetry workflow for surface scanning-tutorial by grzegorz baran. Youtube, 2019. URL <https://www.youtube.com/watch?v=3bGwGpLpSa4>.
- [6] Herbert Bay, Tinne Tuytelaars, and Luc Van Gool. Surf: Speeded up robust features. In Aleš Leonardis, Horst Bischof, and Axel Pinz, editors, *Computer Vision – ECCV 2006*, pages 404–417, Berlin, Heidelberg, 2006. Springer Berlin Heidelberg. ISBN 978-3-540-33833-8.
- [7] Robert C. Burtch. History of photogrammetry. *The Center for Photogrammetric Training*, 2008. URL https://ibis.geog.ubc.ca/courses/geob373/lectures/Handouts/History_of_Photogrammetry.pdf.
- [8] Abraham H. Clark and Robert P. Behringer. Jet-induced 2-D crater formation with horizontal symmetry breaking. *Granular Matter*, 16:433–440, 2014. URL <https://doi.org/10.1007/s10035-014-0501-9>.
- [9] Wyatt C. Million and Carly Kenkel. Image capture and pre-filtering for 3d photogrammetry of coral colonies. *Protocols.io*, 2020. doi: 10.17504/protocols.io.bgdcjs2w. URL <https://par.nsf.gov/biblio/10214896>.
- [10] Evan L. Denmark. *A technical analysis of photogrammetry with Reality Capture*. PhD thesis, Massachusetts Institute of Technology. Department of Electrical Engineering and Computer Science, 2020. URL <https://hdl.handle.net/1721.1/129202>.
- [11] Collins English Dictionary. theodolite. HarperCollins Publishers, 2022. URL <https://www.collinsdictionary.com/dictionary/english/theodolite>.

- [12] Frederick J. Doyle. The historical development of analytical photogrammetry. In *Photogrammetric Engineering*, pages 259–265. The Autometric Corporation, Washington, D.C., 1964.
- [13] Tom Foster. A “good” photo set. *Capturing Reality Support*. URL <https://support.capturingreality.com/hc/en-us/community/posts/360009255471-A-good-photo-set>.
- [14] Grzegorz Gabara and Piotr Sawicki. Accuracy study of close range 3d object reconstruction based on point clouds. pages 25–29, 06 2017. doi: 10.1109/BGC.Gemantics.2017.62.
- [15] Grzegorz Gabara and Piotr Sawicki. A new approach for inspection of selected geometric parameters of a railway track using image-based point clouds. *Sensors (Basel, Switzerland)*, 18, 03 2018. doi: 10.3390/s18030791.
- [16] M. G. Giuliano. Cultural heritage: an example of graphical documentation with automated photogrammetric systems. *The International Archives of the Photogrammetry, Remote Sensing and Spatial Information Sciences*, XL-5:251–255, 2014. doi: :10.5194/isprsarchives-XL-5-251-2014.
- [17] Sharey Guleria and Dhiraj Patil. Experimental investigations of crater formation on granular bed subjected to an air-jet impingement. *Physics of Fluids*, 32:053309, 05 2020. doi: 10.1063/5.0006613.
- [18] Robert Haehnel, W. Dade, and Benoit Cushman-Roisin. Crater evolution due to a jet impinging on a bed of loose particles. pages 1–10, 09 2008. ISBN 978-0-7844-0988-6. doi: 10.1061/40988(323)2.
- [19] Robert B. Haehnel, Benoit Cushman-Roisin, and W. Brian Dade. Cratering by a subsonic jet impinging on a bed of loose particles. *Earth Space*, pages 1–8, 03 2006. doi: 10.1061/40830(188)19.
- [20] Bertil Hallert. Symposium—non-topographic photogrammetry. pages 69–71. 1955.
- [21] Timothy Hanson and Capturing Reality. Getting started with realitycapture with timothy hanson - webinar recording. Youtube, 2020. URL <https://www.youtube.com/watch?v=jeeccnjWIZs&t=1401s>.
- [22] Christopher Immer and Philip Metzger. Rocket cratering in simulated lunar and martian environments. 03 2010. doi: 10.1061/41096(366)20.
- [23] Rob Kesack. Processing in progress: A benchmark analysis of photogrammetry applications for digital architectural documentation. *Technology—Architecture + Design*, 6(1):118–122, 2022. doi: 10.1080/24751448.2022.2040313. URL <https://doi.org/10.1080/24751448.2022.2040313>.
- [24] Kaitlyn Kingsland. A comparative analysis of two commercial digital photogrammetry software for cultural heritage applications. In Marco Cristani, Andrea Prati, Oswald Lanz, Stefano Messelodi, and Nicu Sebe, editors, *New Trends in Image Analysis and Processing – ICIAP 2019*, pages 70–80, Cham, 2019. Springer International Publishing. ISBN 978-3-030-30754-7.

- [25] Kaitlyn Kingsland. Comparative analysis of digital photogrammetry software for cultural heritage. *Digital Applications in Archaeology and Cultural Heritage*, 18:e00157, 2020. ISSN 2212-0548. doi: <https://doi.org/10.1016/j.daach.2020.e00157>. URL <https://www.sciencedirect.com/science/article/pii/S2212054820300564>.
- [26] Klaus Knödel, Gerhard Lange, Hans-Jürgen Voigt, Dietmar Schmidt, Peter Herms, Anke Steinbach, and Friedrich Kühn. *Environmental Geology, Handbook of Field Methods and Case Studies*, chapter 3.2 Photogrammetry. Springer, 2007. ISBN 9783540746690.
- [27] Gotfried Konecny. The international society for photogrammetry and remote sensing—75 years old, or 75 years young. In *Photogrammetric Engineering and Remote Sensing*, chapter Keynote Address, pages 919–933. 1985.
- [28] Ben Kreimer. A guide to photogrammetry photography. *Online News Association*, 2020. URL <https://journalists.org/resources/a-guide-to-photogrammetry-photography/#:~:text=Ensure%20your%20shutter%20speed%20is,re%20steady%20with%20the%20camera>).
- [29] C. Q. LaMarche, J. S. Curtis, and Philip Metzger. Cratering of a lunar soil simulant, jsc-1a, by a turbulent subsonic jet. pages 36–44, 04 2012. ISBN 978-0-7844-1219-0. doi: 10.1061/9780784412190.005.
- [30] Casey LaMarche and Jennifer Curtis. Cratering of a particle bed by a subsonic turbulent jet: Effect of particle shape, size and density. *Chemical Engineering Science*, 138:432–445, 09 2015. doi: 10.1016/j.ces.2015.08.030.
- [31] Stefano Marziali and Giulia Dionisio. Photogrammetry and macro photography. the experience of the musint ii project in the 3d digitizing process of small size archaeological artifacts. *Studies in Digital Heritage*, 1(2):298–309, Dec. 2017. doi: 10.14434/sdh.v1i2.23250. URL <https://scholarworks.iu.edu/journals/index.php/sdh/article/view/23250>.
- [32] Gomer T. McNeil. Some aspects of non-topographic photogrammetry. pages 49–56. 1955.
- [33] Manish Mehta. Rocket plume interactions for nasa landing systems. 2019. URL www.nasa.gov.
- [34] Manish Mehta, Nilton O. Renno, John Marshall, M. Rob Grover, Anita Sengupta, Neal A. Rusche, Jasper F. Kok, Raymond E. Arvidson, Wojciech J. Markiewicz, Mark T. Lemmon, and Peter H. Smith. Explosive erosion during the phoenix landing exposes subsurface water on mars. *Icarus*, 211(1):172–194, 2011. ISSN 0019-1035. doi: <https://doi.org/10.1016/j.icarus.2010.10.003>. URL <https://www.sciencedirect.com/science/article/pii/S0019103510003829>.
- [35] P T Metzger, J E Lane, C D Immer, and S Clements. Cratering and blowing soil by rocket engines during lunar landings. *International Conference on Case Histories in Geotechnical Engineering*, 1, 2008.

- [36] Philip Metzger, Christopher Immer, Carly Donahue, Bruce Vu, Robert Latta III, and Matthew Deyo-Svendsen. Jet-induced cratering of a granular surface with application to lunar spaceports. *Journal of Aerospace Engineering*, 22, 06 2009. doi: 10.1061/(ASCE)0893-1321(2009)22:1(24).
- [37] J. Paul Getty Museum. *The silver canvas: daguerreotype master-pieces from the J. Paul Getty Museum*. Los Angeles: The Museum, 1998.
- [38] Andrzej Pydyn, Mateusz Popek, Maria Kubacka, and Łukasz Janowski. Exploration and reconstruction of a medieval harbour using hydroacoustics, 3-d shallow seismic and underwater photogrammetry: A case study from puck, southern baltic sea. *Archaeological Prospection*, 28(4):527–542, 2021. doi: <https://doi.org/10.1002/arp.1823>. URL <https://onlinelibrary.wiley.com/doi/abs/10.1002/arp.1823>.
- [39] Nicolas Rasmont, Hussein T. Al-Rashdan, Gregory Elliott, Joshua Rovey, and Laura Villafaña Roca. Millimeter wave interferometry for ejecta concentration measurements in plume-surface interactions. AIAA Scitech Forum 2022. American Institute of Aeronautics and Astronautics Inc, AIAA, 2022. doi: 10.2514/6.2022-2421.
- [40] Fabio Remondino, Erica Nocerino, Isabella Toschi, and Fabio Menna. A critical review of automated photogrammetric processing of large datasets. *ISPRS - International Archives of the Photogrammetry, Remote Sensing and Spatial Information Sciences*, XLII-2/W5:591–599, 08 2017. doi: 10.5194/isprs-archives-XLII-2-W5-591-2017.
- [41] Birute Ruzgiene and Edita Alekniene. Analytical and digital photogrammetric geodata production systems (a comparison test). *Geodezija ir Kartografija*, 33(2):50–54, 2007. doi: 10.1080/13921541.2007.9636717. URL <https://www.tandfonline.com/doi/abs/10.1080/13921541.2007.9636717>.
- [42] Josef Sivic and Andrew Zisserman. *Video Google: Efficient Visual Search of Videos*, pages 127–144. Springer Berlin Heidelberg, Berlin, Heidelberg, 2006. ISBN 978-3-540-68795-5. doi: 10.1007/11957959_7. URL https://doi.org/10.1007/11957959_7.
- [43] Daniel Stubbs, Lokesh Silwal, Brian S. Thurow, Masatoshi Hirabayashi, Vishank Raghav, and David Scarborough. *Non-intrusive, 3D Optical Measurements of Crater Formation due to Plume-Surface Interactions*. 2021. doi: 10.2514/6.2021-0831. URL <https://arc.aiaa.org/doi/abs/10.2514/6.2021-0831>.
- [44] Daniel C. Stubbs, Lokesh Silwal, Brian S. Thurow, Masatoshi Hirabayashi, Vishank Raghav, and David E. Scarborough. Three-dimensional measurement of the crater formation during plume–surface interactions using stereo-photogrammetry. *AIAA Journal*, 60(3):1316–1331, 2022. doi: 10.2514/1.J060835. URL <https://doi.org/10.2514/1.J060835>.
- [45] Anuj Tiwari. 15 of the world’s oldest photos that reveal how far we’ve come. *Indiatimes*, 2021. URL <https://www.indiatimes.com/trending/social-relevance/worlds-oldest-photos-543067.html>.

- [46] Styliani Verykokou, Sofia Soile, Fotis Bourexis, Panagiotis Tokmakidis, Konstantinos Tokmakidis, and Charalabos Ioannidis. *A Comparative Analysis of Different Software Packages for 3D Modelling of Complex Geometries*, pages 228–240. 04 2021. ISBN 978-3-030-73042-0. doi: 10.1007/978-3-030-73043-7_19.
- [47] Susan Watanabe and Brian Dunbar. Four out of six apollo, 2008. URL <https://www.nasa.gov/topics/moonmars/features/alhat20081223.html>.
- [48] Robin Wheeler. The fairchild lunar mapping camera. In *The Apollo Scientific Instrument Module (SIM) Cameras*. Apollo Flight Journal, 2017. URL <https://history.nasa.gov/afj/simbaycam/fairchild-lunar-mapping-camera.html>.
- [49] Amanda L. Willingham and Trystan M. Herriott. Photogrammetry-derived digital surface model and orthoimagery of slope mountain, north slope, alaska, june 2018. page 9, 01 2020. doi: 10.14509/30419.
- [50] Paul R. Wolf, Bon A. Dewitt, and Benjamin E. Wilkinson. Introduction to analytical photogrammetry. In *Elements of Photogrammetry with Applications in GIS*, chapter 11. New York: McGraw-Hill Education, 4th edition, . URL <https://www-accessengineeringlibrary-com.proxy2.library.illinois.edu/content/book/9780071761123/chapter/chapter11>.
- [51] Paul R. Wolf, Bon A. Dewitt, and Benjamin E. Wilkinson. Fundamental principles of digital image processing. In *Elements of Photogrammetry with Applications in GIS*, chapter 15. New York: McGraw-Hill Education, 4th edition, . URL <https://www-accessengineeringlibrary-com.proxy2.library.illinois.edu/content/book/9780071761123/chapter/chapter15>.
- [52] Paul R. Wolf, Bon A. Dewitt, and Benjamin E. Wilkinson. Principles of photography and imaging. In *Elements of Photogrammetry with Applications in GIS*, chapter 2. New York: McGraw-Hill Education, 4th edition, . URL <https://www-accessengineeringlibrary-com.proxy2.library.illinois.edu/content/book/9780071761123/chapter/chapter2#/c9780071761123ch02lev1sec12>.
- [53] Paul R. Wolf, Bon A. Dewitt, and Benjamin E. Wilkinson. Introduction. In *Elements of Photogrammetry with Applications in GIS*, chapter 1. New York: McGraw-Hill Education, 4th edition, . URL <https://www-accessengineeringlibrary-com.proxy2.library.illinois.edu/content/book/9780071761123/chapter/chapter1#/c9780071761123ch01lev1sec02>.
- [54] Bo Wu. Photogrammetry:3-d from imagery. 2017. URL http://www.lsgi.polyu.edu.hk/staff/bo.wu/publications/wu_2017_IEG_wbieg0942.pdf.